Electronic Supplementary Material (ESI) for Journal of Materials Chemistry A.

Electronic Supplementary Information.

Thermo-Sensitive Polymer Network Crosslinked by Prussian Blue Nanocrystals for Cesium Adsorption from Aqueous Solution with Large Capacity

Jun Qian [a], *Suya Cai* [a], *Sen Yang* [b], *Daoben Hua* [a,b] *

[a] School for Radiological and Interdisciplinary Sciences (RAD–X) & College of Chemistry, Chemical Engineering and Materials Science, Soochow University, Suzhou 215123, China

[b] Collaborative Innovation Center of Radiological Medicine of Jiangsu Higher Education Institutions, Suzhou 215123, China

CORRESPONDING AUTHOR FOOTNOTE.

Dr. D. Hua

School for Radiological and Interdisciplinary Sciences (RAD–X), Soochow University, Suzhou 215123, China

Tel: (+) 86–512–65882050; Fax: (+) 86–512–65883261; E–mail: dbhua_lab@suda.edu.cn

Table of contents

1. Characterization methods

Elemental analysis was determined on an ELEMENTAR CHNOS Elemental Analyzer. Thermogravimetric analysis (TGA) was performed on TG/DTA 6300 in a N_2 flow. Z-average size distribution was determined by Malvern Zetasizer with irradiation (He–Ne laser, 632.8 nm). ^{1}H NMR and ^{13}C NMR spectra were recorded on a Varian INVOA-400 instrument working at 400 MHz. Fourier transform infrared (FT-IR) spectra were recorded by Varian-1000 spectrometer. Energy-dispersive X-ray (EDX) analysis was carried out by a Hitachi S570 scanning electron microscope. Transmission electron microscopy (TEM) images were taken with a FEI Tecnai G20 electron microscope (accelerating voltage, 200 kV). Powder X-ray diffraction (XRD) data were collected from 5 to 80 ° with a step of 0.02 ° and the time for data collection was 0.5 s on a Bruker D8 Advance diffractometer with Cu Kα radiation (λ = 1.54056 Å). X-ray photoelectron spectroscopy (XPS) was carried out by ESCALAB 250Xi XPS. The concentration of cesium ions was determined by using Thermo ELEMENT 2 Inductively Coupled Plasma-Mass Spectrometry (ICP-MS). Zeta potential of composite was determined by Malvern Zetasizer with irradiation (He–Ne laser, 632.8 nm).

2. Synthesis of pentacyano(4-vinyl pyridine)ferrate

Sodium pentacyanoaminoferrate was synthesized according to a modified literature method[1]: sodium pentacyanonitrosylferrate(III) dehydrate (9 g, 17.08 mmol) was dissolved in 80 mL $NH_3 \bullet H_2O$ in ice-bath. Blood red solution was obtained. Then the reaction was allowed to proceed at -7 °C for 18 h. Afterwards, the mixture was filtered and washed with methanol. Then the obtained bright yellow solid was dissolved with ice water and precipitated by dropping into methanol. The needle-like bright yellow crystal was collected and was washed with methanol and was dried under vacuum for 12 h.

Pentacyano(4-vinyl pyridine)ferrate was prepared via a typical process[2]: sodium pentacyanoaminoferrate (2.16 g, 6.6 mmol), hydroquinone (0.06 g, 0.54 mmol) and 4-vinyl pyridine (2.12 mL, 20 mmol) were added to methanol (200 mL). Suspension was stirred overnight yielding a dark red solution at 313.15K. The solution was concentrated under reduced pressure to 30 mL and precipitated by dropping into chloroform. The dark green solid was collected, washed with diethyl ether and was dried under vacuum for 12 h.

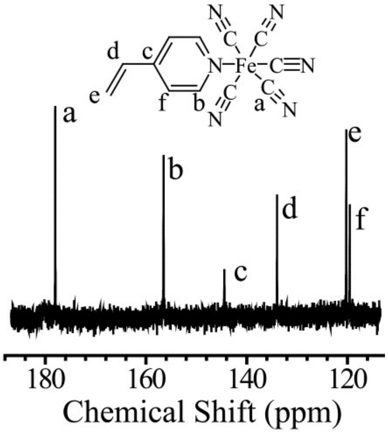

Figure S1. ^{13}C NMR spectrum (D_2O, 400 MHz) of pentacyano(4-vinyl pyridine)ferrate.

3. Synthesis of PB-PNIPAM

P(PVPF-*co*-NIPAM) was synthesized by radical polymerization in solution. Considering the property of LCST, PVPF (0.318 g, 0.75 mmol), NIPAM (0.198 g, 1.75 mmol) and APS (0.03 g, 0.13 mmol) were dissolved in mixed solution of deionized water and acetone (v/v = 1/1, 8 mL). And then, the solution was deoxygenated by purging with argon gas for 15 min. Subsequently, the mixture was polymerized at 70 °C under argon atmosphere for 72 h. After polymerization, the product was purified by dialysis in deionized water to remove unreacted monomers. And then, excess $FeCl_3\cdot 6H_2O$ was added to deionized water to react with P(PVPF-*co*-NIPAM) to form PB-PNIPAM. Finally, the product was purified by dialysis in deionized water to remove excess Fe^{3+} and lyophilized for 12 h.

4. Calculation of reactivity ratios

$$y = dm_1 / dm_2 \qquad (1)$$

Where dm_1/dm_2 stands for instantaneous monomer ratio in the copolymer formed.

$$z = \frac{\log(m_1 / m_1^0)}{\log(m_2 / m_2^0)} \qquad (2)$$

Where m_1 and m_2 denote concentrations of the two monomers and the superscript zero stands for the initial value of monomer concentration.

$$F = y/z^2 \qquad (3)$$

$$\alpha = \sqrt{F_{\min} F_{\max}} \qquad (4)$$

Where $F_{\min}$ and $F_{\max}$ are the lowest and highest values of F, respectively.

$$\xi = y/(\alpha z^2 + y) \qquad (5)$$

$$\eta = z(y-1)/(\alpha z^2 + y) \qquad (6)$$

$$\eta = (r_1 + \frac{r_2}{\alpha})\xi - \frac{r_2}{\alpha} \qquad (7)$$

Where r_1 and r_2 stand for reactivity ratios of the two monomers. r_1 and r_2 can be determined from the slope and intercept of the plot of η *versus* ξ, respectively.

According the data in Table 2 in the text, several parameters (y, z, F, α, ξ and η) can be calculated. The results are summarized in Table S1.

Table S1. Parameters for copolymerization of VPFC and SBMA[a].

Sample	y	z	F	ξ	η
P(PVPF$_{10}$-*co*-SBMA$_{90}$)	0.368	4.819	0.016	0.060	-0.500
P(PVPF$_{30}$-*co*-SBMA$_{70}$)	0.730	2.247	0.144	0.370	-0.307
P(PVPF$_{40}$-*co*-SBMA$_{60}$)	0.852	1.591	0.336	0.577	-0.160
P(PVPF$_{50}$-*co*-SBMA$_{50}$)	1.033	1.075	0.894	0.784	0.027
P(PVPF$_{60}$-*co*-SBMA$_{40}$)	1.268	0.576	3.826	0.940	0.114

[a] $\alpha = (F_{\min} F_{\max})^{1/2} = 0.246$.

Figure S2 displays the plot of the obtained results and the linear fit, which can be used to calculate both reactivity ratios. The plot reveals that the dependence of η on ξ is linear as indicated by the R^2 parameter ($R^2 = 0.9936$). The reactivity ratios were determined from the linear regression: $r_1 = 0.16$ and $r_2 = 0.14$.

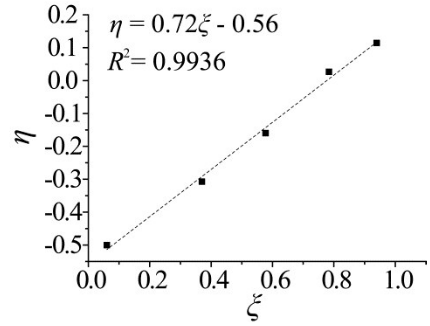

Figure S2. η *versus* ξ plot ($\alpha = 0.246$).

5. Calculation of molar percent of SBMA in the copolymer

According to literature, thermal degradation of poly(sulfobetaine methacrylate) (PSBMA) occurs around 200 °C - 700 °C [3]. And the part of crystal water comes from the solvent of polymerization, which should be deducted. So, molar percent of SBMA in the copolymer (SBMA mol%) could be calculated by Equation (8):

SBMA mol% = m(SBMA)/275/(m(SBMA)/275+ m(PVPF)/424)×100 (8)

Where m(SBMA) and m(PVPF) are the weights of SBMA and VPFC, respectively, which could be obtained from TGA data. The molar weights of SBMA and PVPF are 275 and 424, respectively.

6. Adsorption thermodynamics [4]

$$K_c = q_e/c_e \qquad (9)$$

$$\ln K_c = \frac{\Delta S}{R} - \frac{\Delta H}{RT} \qquad (10)$$

$$\Delta G = -RT \ln K_c \qquad (11)$$

Where R and T are the ideal gas constant (8.314 J/mol/K) and the absolute temperature, respectively. ΔH and ΔS can be obtained from the slope and intercept of the plot of $\ln K_c$ versus $1/T$.

7. Adsorption kinetics

Pseudo-first-order kinetic equation describes the relationship between the adsorption rate and adsorption amount q_t at time t [5]:

$$\log(q_e - q_t) = \log q_e - (\frac{k_1}{2.303}) \times t \qquad (12)$$

Where k_1 (h^{-1}) is the pseudo first order kinetic constant. k_1 and q_e can be determined from the slope and intercept of the plot of log (q_e-q_t) versus t, respectively (Figure S7A).

Pseudo-second-order model is expressed as the following Equation (13) [6, 7]:

$$\frac{t}{q_t} = \frac{1}{k_2 \times q_e^2} + \frac{t}{q_e} \qquad (13)$$

Where k_2 (g/mg/h) is the second order rate constant. If the plot of t/q_t versus t shows a linear relationship, k_2 and q_e can be determined from the slope and intercept of the line (Figure S7B).

8. Adsorption isotherm

Langmuir model is given as Equation (10), which describes monolayer adsorption based on the assumption that all the adsorption sites have equal affinity, and that desorption at one site doesn't affect an adjacent site [8].

$$\frac{1}{q_{\mathrm{e}}} = \frac{1}{q_{\max} b c_{\mathrm{e}}} + \frac{1}{q_{\max}} \qquad (14)$$

Error!Where $q_{\max}$ (mg/g) is the maximum adsorption amount (i.e. adsorption capacity), and b (L/mg) is the Langmuir constant. They can be calculated from the linear plot of c_e/q_e against c_e (Figure S8A).

The Freundlich model can be applied for multilayer adsorption and the adsorption on heterogeneous surfaces[9], which can be expressed as Equation (11):

$$\log q_{\mathrm{e}} = \log K_{\mathrm{F}} + \frac{1}{\mathrm{n}} \log c_{\mathrm{e}} \qquad (15)$$

Where K_F (L/g) and n are Freundlich constants related to adsorption capacity and adsorption intensity, respectively, which can be calculated from the linear plot of log q_e versus log c_e (Figure S8B).

9. Calculation of cell parameters

Interplanar spacing can be calculated according to Bragg equation: $2d \sin \theta = n \lambda$, where d stands for interplanar spacing, θ is the angle between the incident X ray and the corresponding crystal surface, n (1) is diffraction series and λ (1.54056 Å) means the wavelength of incident X ray.

In this work, interplanar spacing before and after adsorption were obtained as $d_{\mathrm{before}} = 5.074$ Å, and $d_{\mathrm{after}} = 4.991$ Å, respectively.

Prussian blue is a fcc crystal structure, so $d = a / (h^2+k^2+l^2)^{1/2}$, where a stands for cell parameter, and h, k, l are Miller index.

Therefore, a from (100) XRD signal before and after adsorption in this study can be calculated as $a_{\mathrm{before}} = 5.074$ Å, and $a_{\mathrm{after}} = 4.991$ Å, respectively.

Table S2. Thermodynamic data for cesium adsorption by Prussian blue.

ΔH (kJ/mol)	ΔS (J/mol K)	ΔG (kJ/mol)			
		286.15K	308.15K	318.15K	328.15K
46.78	163.26	-0.59	-2.35	-4.27	-8.21

Table S3. Comparison of cesium adsorption capacities of composite with other PB based materials.

Matrix	Capacity (mg/g)	Reference
Prussian blue based nanocomposites (FPPB)	72.5	[10]
Magnetic Prussian blue/graphene oxide nanocomposites caged in calcium alginate microbeads	40.8	[11]
Magnetic Prussian blue nanocomposites	280.8	[12]
Magnetic Prussian blue (MPB)	347.0	[13]
Magnetic Prussian blue graphene oxide (MPBGO)	362.0	[13]
Prussian blue analog caged in chitosan surface-decorated carbon nanotubes (PBA/CS/CNTs)	219.8	[14]
Cellulose nanofiber backboned Prussian blue nanoparticles	139	[15]
Prussian blue functionalized graphene/carbon fibers composite	81.2	[16]
Pectin-stabilized magnetic graphene oxide Prussian blue nanocomposites (PSMGPB)	424.3	[17]
PB-10	319.5	This work
PB-30	359.7	This work
PB-40	465.1	This work

Table S4. The isotherm parameters for cesium adsorption by PB-PSBMA. (Experiment conditions: 0.13 g/L adsorbent, 3 mL solution, pH 7.0, 50 ^{o}C. mean ± SD, n = 3)

Adsorbent	Langmuir			Freundlich		
	q_{max} (mg/g)	b (L/mg)	R^2	K_F (L/g)	n	R^2
PB-10	561.8	0.0031	0.997	8.12	1.69	0.990
PB-30	671.1	0.0027	0.997	7.84	1.62	0.978
PB-40	680.3	0.0033	0.996	10.7	1.72	0.983

Table S5. The diameter and charge-to-radius ratio of ions.

Ion	Ion diameter (Å) [18, 19]	Stokes diameter (Å) [18, 19]	Charge-to-radius ratio[a]
Cs^+	3.72	2.38	0.84
K^+	2.66	2.50	0.80
Na^+	1.90	3.68	0.54
Ca^{2+}	1.98	6.20	0.65
Mg^{2+}	1.30	6.94	0.58
Mn^{2+}	1.60	7.36	0.54
Co^{2+}	1.44	6.70	0.60
Ni^{2+}	1.40	5.84	0.68
Cu^{2+}	1.44	6.50	0.62
Zn^{2+}	1.48	6.98	0.57
Sr^{2+}	2.26	6.20	0.65
Cd^{2+}	1.94	6.82	0.59
Ba^{2+}	2.70	5.80	0.69
Cr^{3+}	1.28	8.24	0.73

a: Calculated by equation: Charge-to-radius ratio = Charge number/ Stokes radius.

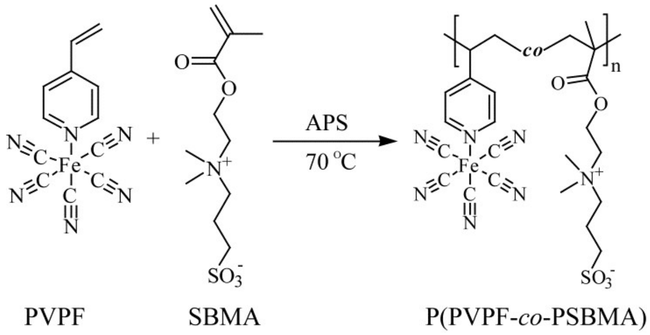

Scheme S1. Synthesis of P(PVPF-*co*-SBMA) copolymers via radical polymerization.

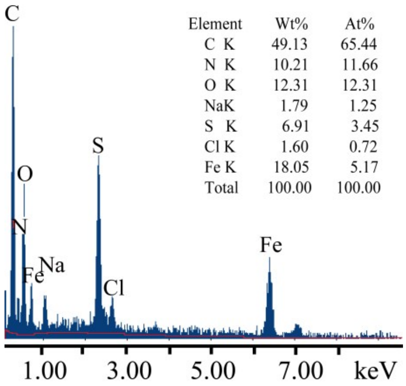

Element	Wt%	At%
C K	49.13	65.44
N K	10.21	11.66
O K	12.31	12.31
NaK	1.79	1.25
S K	6.91	3.45
Cl K	1.60	0.72
Fe K	18.05	5.17
Total	100.00	100.00

Figure S3. EDX spectrum of P(PVPF-*co*-SBMA).

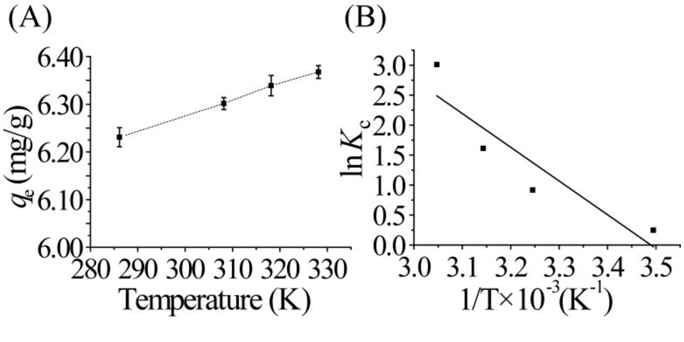

Figure S4. (A) Effect of temperature on the adsorption of cesium ions by Prussian blue, and (B) plots of lnK_c *versus* 1/T for Prussian blue. (Experimental conditions: 3 mL solution, 1 ppm cesium ion, 0.13 g/L adsorbents, pH 7.)

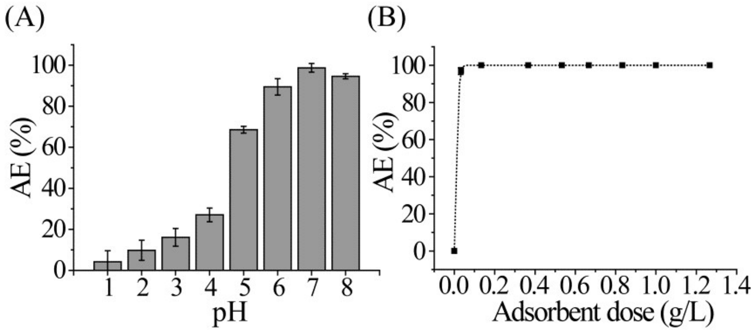

Figure S5. Effect of (A) pH and (B) adsorbent dose on adsorption efficiency (AE) of cesium ions by PB-PSBMA. (Experimental conditions: 3 mL solution, 1 ppm cesium ion, pH 7, 50 ^{o}C.)

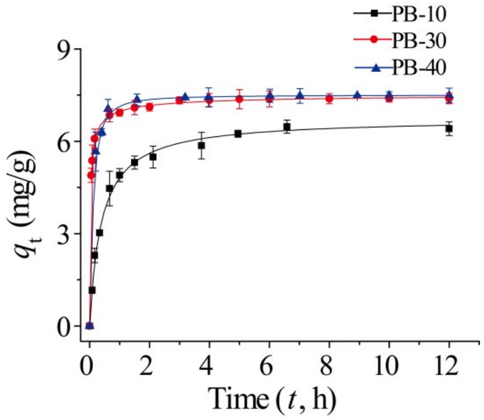

Figure S6. Effect of contact time on the adsorption of cesium ions by PB-10, PB-30, and PB-40. (Experimental condition: 3 mL solution, 1 ppm cesium ion, 0.13 g/L adsorbents, pH 7, and 50 ^{o}C. mean ± SD, n = 3)

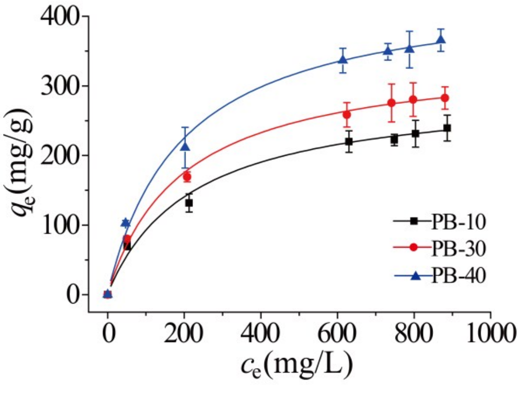

Figure S7. Adsorption isotherm plots for cesium adsorption by PB-10, PB-30, and PB-40. (Experiment conditions: 0.13 g/L adsorbent, 3 mL solution, pH 7.0, 30 ^{o}C. mean ± SD, n = 3)

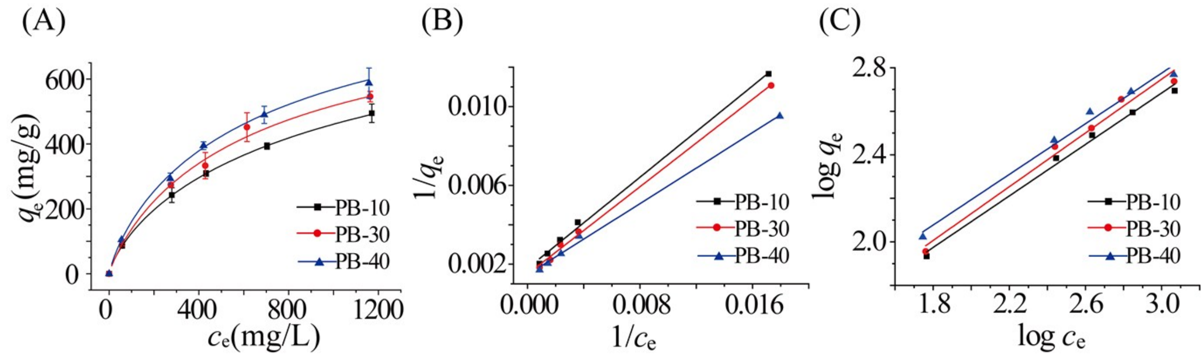

Figure S8. (A) Adsorption isotherm plots (B) Langmuir isotherm and (C) Freundlich isotherm plots for cesium adsorption by PB-10, PB-30, and PB-40. (Experiment conditions: 0.13 g/L adsorbent, 3 mL solution, pH 7.0, 50 °C. mean ± SD, n = 3)

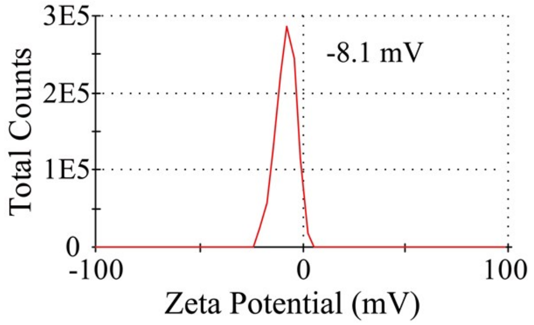

Figure S9. Zeta potential of PB-PSBMA.

Reference

1. Kenney, D.; Flynn, T.; Gallini, J., Reactions of ferropentacyanamines. *Journal of Inorganic and Nuclear Chemistry* **1961,** *20* (1), 75-81.

2. Qian, J.; Ma, J.; He, W.; Hua, D., Facile Synthesis of Prussian Blue Derivate-Modified Mesoporous Material via Photoinitiated Thiol-Ene Click Reaction for Cesium Adsorption. *Chemistry-an Asian Journal* **2015,** *10* (8), 1738-1744.

3. Lalani, R.; Liu, L., Synthesis, characterization, and electrospinning of zwitterionic poly(sulfobetaine methacrylate). *Polymer* **2011,** *52* (23), 5344-5354.

4. Sarı, A.; Tuzen, M.; Soylak, M., Adsorption of Pb (II) and Cr (III) from aqueous solution on Celtek clay. *Journal of Hazardous Materials* **2007,** *144* (1), 41-46.

5. Lagergren, S., zur theorie der sogenannten adsorption gelöster stoffe. *K. Sven. Vetenskapsakad., Handl.,*

Band 24 **1898,** *4*, 1-39.

6. Ho, Y.-S.; McKay, G., Sorption of dye from aqueous solution by peat. *Chemical Engineering Journal* **1998,** *70* (2), 115-124.
7. Ho, Y. S., Review of second-order models for adsorption systems. *Journal of Hazardous Materials* **2006,** *136* (3), 681-689.
8. Langmuir, I., The constitution and fundamental properties of solids and liquids Part I Solids. *Journal of the American Chemical Society* **1916,** *38*, 2221-2295.
9. Freundlich, H., Concerning adsorption in solutions. *Zeitschrift Fur Physikalische Chemie--Stochiometrie Und Verwandtschaftslehre* **1906,** *57* (4), 385-470.
10. Yang, H.; Li, H.; Zhai, J.; Yu, H., In situ growth of Prussian blue nanocrystal within Fe3+ crosslinking PAA resin for radiocesium highly efficient and rapid separation from water. *Chemical Engineering Journal* **2015,** *277*, 40-47.
11. Yang, H.; Li, H.; Zhai, J.; Sun, L.; Zhao, Y.; Yu, H., Magnetic prussian blue/graphene oxide nanocomposites caged in calcium alginate microbeads for elimination of cesium ions from water and soil. *Chemical Engineering Journal* **2014,** *246*, 10-19.
12. Jang, J.; Lee, D. S., Magnetic Prussian Blue Nanocomposites for Effective Cesium Removal from Aqueous Solution. *Industrial & Engineering Chemistry Research* **2016,** *55* (13), 3852-3860.
13. Lujaniene, G.; Semcuk, S.; Lecinskyte, A.; Kulakauskaite, I.; Mazeika, K.; Valiulis, D.; Pakstas, V.; Skapas, M.; Tumenas, S., Magnetic graphene oxide based nano-composites for removal of radionuclides and metals from contaminated solutions. *Journal of Environmental Radioactivity* **2017,** *166*, 166-174.
14. Li, T.; He, F.; Dai, Y., Prussian blue analog caged in chitosan surface-decorated carbon nanotubes for removal cesium and strontium. *Journal of Radioanalytical and Nuclear Chemistry* **2016,** *310* (3), 1139-1145.
15. Vipin, A. K.; Fugetsu, B.; Sakata, I.; Isogai, A.; Endo, M.; Li, M.; Dresselhaus, M. S., Cellulose nanofiber backboned Prussian blue nanoparticles as powerful adsorbents for the selective elimination of radioactive cesium. *Scientific Reports* **2016,** *6*.
16. Chen, F.-P.; Jin, G.-P.; Peng, S.-Y.; Liu, X.-D.; Tian, J.-J., Recovery of cesium from residual salt lake brine in Qarham playa of Qaidam Basin with prussian blue functionalized graphene/carbon fibers composite. *Colloids and Surfaces a-Physicochemical and Engineering Aspects* **2016,** *509*, 359-366.
17. Kadam, A. A.; Jang, J.; Lee, D. S., Facile synthesis of pectin-stabilized magnetic graphene oxide Prussian blue nanocomposites for selective cesium removal from aqueous solution. *Bioresource Technology* **2016,** *216*, 391-398.
18. Volkov, A. G.; Paula, S.; Deamer, D. W., Two mechanisms of permeation of small neutral molecules and hydrated ions across phospholipid bilayers. *Bioelectrochemistry and Bioenergetics* **1997,** *42* (2), 153-160.
19. Nightingale, E. R., Phenomenological theory of ion solvation - effective radii of hydrated ions. *Journal of Physical Chemistry* **1959,** *63* (9), 1381-1387.